Civil Engineering Infrastructures Journal xx,xx
DOI: 10.22059/CEIJ.2023.356871.1917

Seismic Assessment of Base-Isolated Structure Under a Sequence of Near-Fault Earthquake Records

Isam Yousef[1], Mohammad Al-Nawaiseh[2], Mohammad Al-Rawashdeh[3, *]

[1] Assistant Professor, Department of Civil Engineering, Munib and Angela Masri Faculty of Engineering, Aqaba University of Technology, Aqaba 77110, Jordan. (Email: isharkas@aut.edu.jo)

[2]Assistant Professor, Department of Civil Engineering, Faculty of Engineering, Amman Arab University, Amman 11118, Jordan. (Email: m.nawaiseh@aau.edu.jo)

[3] Assistant Professor, Department of Civil Engineering, Faculty of Engineering, Al-Balqa Applied University, Al-Salt 19117, Jordan. (Email: dr_alrawashdeh@bau.edu.jo)

*Corresponding author: (Email: dr_alrawashdeh@bau.edu.jo; Phone: 00962790122380)

Conflicts of Interest

On behalf of all the authors, the corresponding author states that there is no conflict of interest.

Funding

The authors declare that they have not received any funding for this paper.

Data Availability Statement

The data presented in this study are available on request from the corresponding author.

Author Contributions

Conceptualization, Isam Yousef, Mohammad Al-Nawaiseh, Mohammad Al-Rawashdeh; ***Methodology***, Isam Yousef, Mohammad Al-Nawaiseh; ***Investigation***, Isam Yousef, Mohammad Al-Nawaiseh, Mohammad Al-Rawashdeh; ***Writing—original draft preparation***, Isam Yousef, Mohammad Al-Nawaiseh; ***Writing—review and editing***, Mohammad Al-Rawashdeh; ***Visualization***, Isam Yousef, Mohammad Al-Nawaiseh, Mohammad Al-Rawashdeh.

All authors have read and agreed to the published version of the manuscript.

Received: 16/03/2023
Revised: 06/08/2023
Accepted: 14/08/2023

Abstract

This paper investigates the performance and efficacy of quintuple friction pendulum (QTFP) isolators under a sequence of near-fault foreshock, mainshock, and aftershock earthquake events. The QTFP isolator is an advanced base isolation device utilized in reinforced concrete (RC) structures to alleviate damage from severe seismic activity. Despite its proven ability to restrict structural responses and meet particular performance goals under severe seismic excitation, comprehensive analyses of QTFP isolators' performance under sequential earthquakes are scarce. This research employs finite element analysis to explore the seismic behavior of RC structures equipped with QTFP isolators during such sequences. It also assesses the effectiveness of QTFP isolators by evaluating the seismic behavior of base-isolated RC structures subjected to sequence earthquakes. In general, the sequence of foreshock, mainshock, and aftershock earthquake events critically impacts the structural response, with the foreshock producing the highest base shear, inter-story drift, and acceleration responses. Furthermore, the aftershock accounted for the most considerable input, damping, and hysteretic energies. The research offers insights into the hysteresis behavior of the isolators, particularly during the mainshock, where the combination of 2.15 seconds period and 10% damping showcased the most extensive hysteresis loop cycles. This study underscores the significance of QTFP isolators in enhancing the seismic resistance of RC structures, while shedding light on their performance under different earthquake sequences.

Keywords: Reinforced concrete, low-rise structure, multi-staged friction pendulum isolators, sequence of near-fault earthquake, nonlinear response history analysis.

1. Introduction

The seismic mitigation of RC structures subjected to strong earthquakes, which may result in a partial or total collapse of the building, has been the interest of many studies(Mesr and Behnamfar, 2023; Nallasivam, 2023). Implementing a base isolation system proved to be an efficient and effective technique for reducing seismic damage by enhancing the structure's resilience and providing an overall safety performance in contrast with fixed-base structures (Gandelli, 2017). This can be achieved via alteration of the fundamental period of the building and enhancement of the energy dissipation capacity resulting in lower transmitted energy and hence lower structural responses such as displacement and acceleration (Sodha et al., 2017; Keikha and Ghodrati Amiri, 2021). In general, base isolation systems implemented for seismic protection of RC structures can be categorized into rubber isolators and frictional sliding isolators. Within the group of frictional sliding isolators, flat sliding isolators and friction pendulum isolators are the most used devices. Friction pendulum isolators group includes single friction pendulum (SFP), double friction pendulum (DFP), triple friction pendulum (TFP), and quintuple friction pendulum (QTFP). In general, a multi-staged friction isolation system leverages multiple points of energy dissipation to significantly reduce the propagation of mechanical vibrations or shocks. This method essentially uses multiple friction interfaces that convert mechanical energy into heat through friction, mitigating vibration transmission. The advantage of this system lies in its capability to handle complex or varying energy inputs, as each stage can deal with different energy levels or frequencies. This multi-staged approach distributes the isolation task, preventing any single stage from being overwhelmed. Consequently, it enhances system resilience, ensuring overall stability and protection for sensitive equipment from potentially damaging forces. In effect, they improve energy dissipation and reduce maintenance costs. With their robustness and enhanced efficiency, multi-staged friction bearings are a valuable choice for high-performance systems. The SFP isolator consists of a single sliding surface and one pendulum (Zayas et al., 1987; Mokha et al., 1991). The DFP isolator consists of three sliding regimes and two pendula which minimize the heating effects and improve the capacity of displacement (Fenz and Constantinou, 2006). The TFP isolator consists of five sliding regimes and three pendula which

exhibit the same performance as DFP with better-enhanced adaptability of behavior (Dhankot and Soni, 2017; Sodha et al., 2017). Naderpour et al. (2019) presented an insightful investigation into the seismic response of high-rise structures, utilizing innovative methods such as base isolation and non-traditional tuned mass dampers. A different approach was adopted by Sharbatdar et al. (2011), whose work focused on studying the effects of near fault ground motions on base-isolated structures with lead rubber bearings (LRB) and SFP. Meanwhile, Mirrashid and Naderpour (2021) made significant strides in the realm of computational intelligence, offering an advanced model for the vulnerability assessment of RC frames under seismic sequences, hence providing a key resource for further seismic research. The QTFP isolator consists of nine sliding regimes and five pendula, considered the extended version of the TFP isolator (Lee and Constantinou, 2016). In addition, the number of sliding regimes and pendula improves the capacity of adaptive behavior, decreases the heat originating from friction, and improves the displacement capacity as well as the difficulty in modeling the behavior of the devices. Indeed, the QTFP isolator device was introduced and investigated by Tsai et al. (2010), where the force-displacement relationship applicable for the loading phase and model of plastic behavior was performed. This article explores the importance and implications of a pioneering study concerning the QTFP isolator, a sophisticated device employed in RC structures to mitigate the damage caused by severe seismic activities. The significance of this research lies in its potential to drastically improve the resilience of these structures during seismic events and contribute substantially to the field of earthquake engineering. While the QTFP isolator has demonstrated efficacy in limiting structural responses and achieving specific performance objectives under severe seismic excitation, a comprehensive analysis of its performance under a series of near-fault foreshock, mainshock, and aftershock events remains unexplored. This study, therefore, strives to fill this gap in the existing literature and aims to understand the performance and efficiency of RC structures equipped with QTFP isolators under such seismic sequences. Specifically, the study will utilize finite element analysis as a crucial tool to investigate the seismic behavior of RC structures with QTFP isolators during sequential earthquakes. Additionally, the effectiveness of the QTFP isolator will be

analyzed by assessing the seismic behavior of base-isolated RC structures subjected to sequence earthquakes. The potential implications of this study are far-reaching. If successful, it could provide key insights into the effectiveness of the QTFP isolator in mitigating seismic damage, potentially revolutionizing our current understanding of structural design in earthquake-prone areas. This could lead to safer and more resilient infrastructures, significantly reducing both human casualties and economic losses associated with seismic events. This is why the understanding and dissemination of this study are essential, as its findings could serve as a cornerstone for future earthquake engineering research.

2. Materials and Methods

The selection of low-rise RC moment resisting frames representing typical buildings was conducted within this paper, as illustrated in Figure 1. An investigation of the seismic behavior of RC structures equipped with a multi-staged friction pendulum isolator was performed to evaluate the efficiency of the base isolation system under the effect of a sequence of near-fault earthquakes where the bare structure is set to be the benchmark.

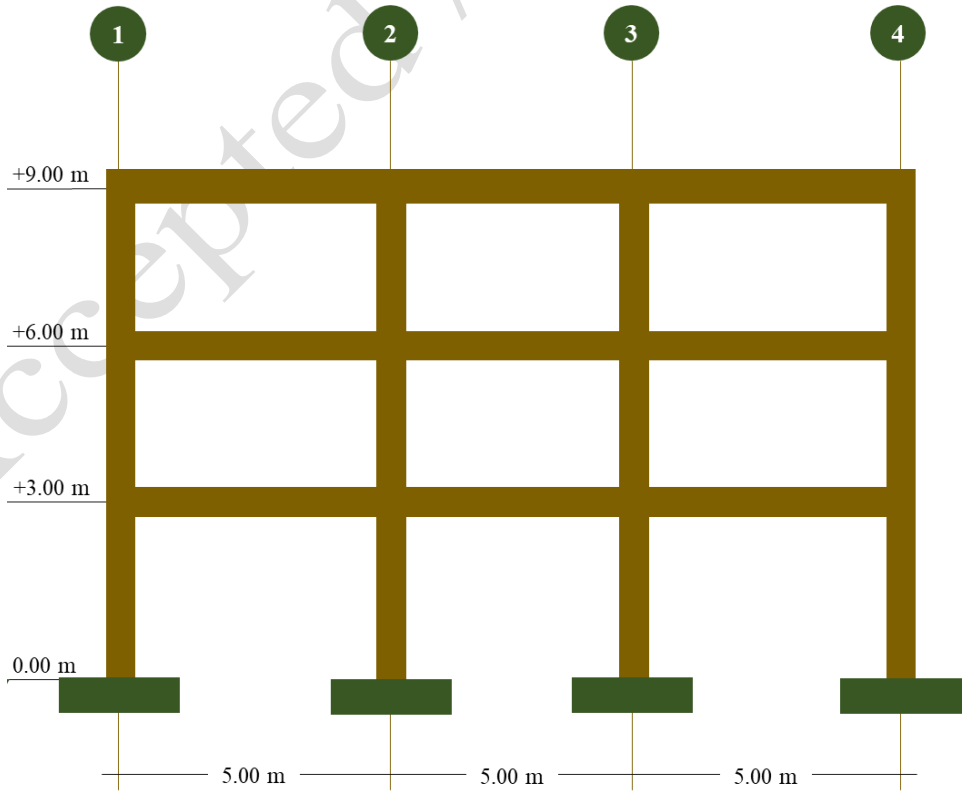

Figure 1: Selected frame structure

QTFP isolator consists of six concave surfaces coated by a Teflon slider, as represented in Figure 2. The change of strength and stiffness of the QTFP isolator corresponds to the direct proportional increase in displacement. The different number of sliding surfaces of the QTFP isolator is accompanied by the increase in complexity in force-deformation performance regarding other friction isolator devices (Sodha et al., 2017). Furthermore, the curve of the force-deformation relationship of the QTFP isolator is composed of nine operating stages, as shown in Figure 3 (Keikha and Ghodrati Amiri, 2021). QTFP isolator can operate in two different design configurations depending on the coefficient of friction magnitudes; where the first configuration is composed of the following: $\mu_3 = \mu_4 < \mu_5 \leq \mu_2 < \mu_6 \leq \mu_1$ while the second configuration is $\mu_3 = \mu_4 < \mu_2 \leq \mu_5 < \mu_6 \leq \mu_1$. Moreover, the difference between the two configurations is the switch of operating stages between 2-3 and 8-9 resulting in slight variation in the loop. Nonetheless, the QTFP isolator possesses one design configuration depending on the effective radius of curvature, which is composed of the following $L_3 = L_4 \ll L_2 \leq L_5 \ll L_1 \leq L_6$ where $L_i = R_i - h_i$. In addition to that, QTFP isolator is governed by the property of geometry which is $d_i^* = d_i \frac{L_i}{R_i}$ where R_i= radius of curvature, d_i=displacement capacity, and h_i=height of ith surface. The simultaneous motion in operating stages 3 and 4 begins in the case of $\mu_3 = \mu_4$ and $L_3 = L_4$ where any change in this case can lead to undetected irregular performance by the presented model and increase in complexity demand (Sarlis and Constantinou, 2013). The frictional forces in each element of the QTFP isolator are in accordance with an extended model by (Constantinou et al., 1990) as the following:

$$F_1 = \bar{\mu}_1(m_b + M)gZ_1 \quad \text{Eq. 1}$$

$$F_2 = \bar{\mu}_2(m_b + m_{s1} + M)gZ_2 \quad \text{Eq. 2}$$

$$F_3 = \bar{\mu}_3(m_b + m_{s1} + m_{s2} + M)gZ_3 \quad \text{Eq. 3}$$

$$F_4 = \bar{\mu}_4(m_b + m_{s1} + m_{s2} + m_{s3} + M)gZ_4 \quad \text{Eq. 4}$$

$$F_5 = \bar{\mu}_5(m_b + m_{s1} + m_{s2} + m_{s3} + m_{s4} + M)gZ_5 \quad \text{Eq. 5}$$

where Z_i is the hysteretic element meeting the requirement of the following nonlinear differential equation:

$$q\frac{dZ_i}{dt} = A\dot{x}_i - \beta|\dot{x}_i||Z_i|^{n-1} - \gamma\dot{x}_i|Z_i|^n \qquad \text{Eq. 6}$$

where q is the displacement quantity while A, β, n, and γ are the dimensionless factors of the hysteresis loop.

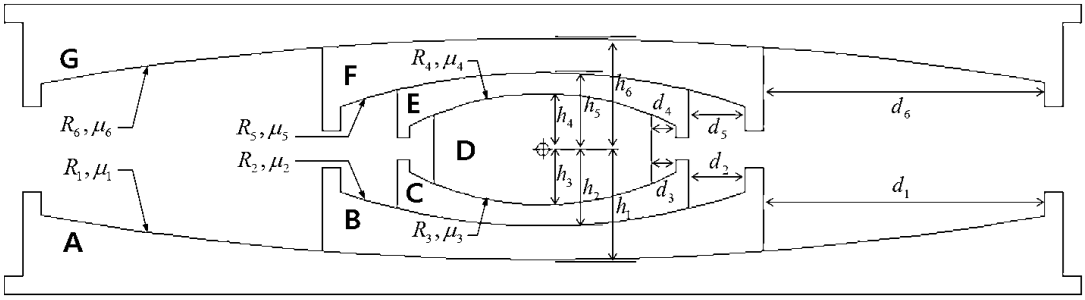

Figure 2: Demonstration of QTFP isolator as introduced by Lee and Constantinou (Lee and Constantinou, 2016)

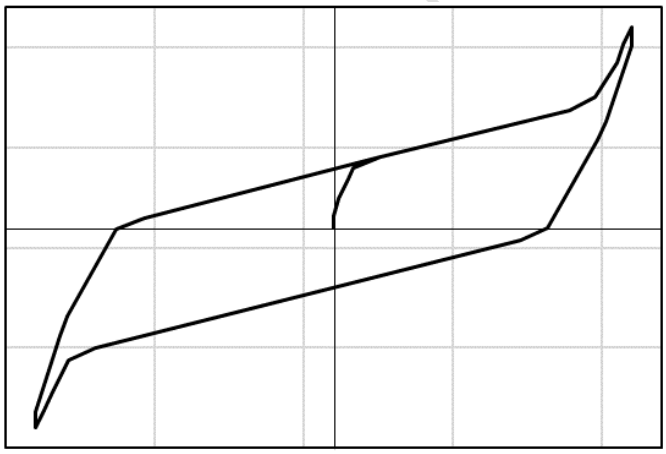

Figure 3: Backbone curve and hysteresis loop of QTFP isolator

In this study, the model used for defining the QTFP is an equivalent approach to the one shown in Figure 4, employing a series of TFP and DFP. Moreover, the isolator's effective stiffness was calculated, as shown in Figure 5, using the method described by Sodha et al. (2017). Lastly, for the aim of conducting this study, three cases of the period were selected, which are 2.15 seconds, 2.68 seconds, and 3 seconds along with damping ratios of 10%, 20%, and 30%, respectively, In general, the displacement requirement of the isolators was first selected based on the requirements of the ASCE 7-16. Since the displacement is the major parameter that physically restrict the isolator from

being used (since in many cases it is not possible to provide an isolator with high displacement capacity because there are limitations coming from nearby structures), the same design and ultimate displacements were used in all cases and then three different cases of isolator with significant differences were select as a way to simulate a real case of discuss the effect of the properties on the response of the building.The properties of the QTFP isolator are illustrated in Table 1.

Table 1: Selected isolator properties

T2.15-ξ10				T2.68-ξ20				T3-ξ30			
R	μ	h	d	R	μ	h	D	R	μ	h	D
0.85	0.11	0.15	0.34	1.5	0.11	0.15	0.32	3	0.14	0.15	0.31
0.55	0.09	0.1	0.1	0.55	0.06	0.1	0.1	0.8	0.065	0.1	0.08
0.3	0.01	0.05	0.03	0.3	0.02	0.05	0.02	0.3	0.02	0.05	0.02
0.3	0.01	0.05	0.03	0.3	0.02	0.05	0.02	0.3	0.02	0.05	0.02
0.55	0.08	0.1	0.1	0.55	0.05	0.1	0.1	0.8	0.05	0.1	0.08
0.85	0.1	0.15	0.34	1.5	0.09	0.15	0.32	3	0.11	0.15	0.31

The frame structure shown in Figure 1 was designed, and the selected beams and columns sections for the building were 0.4 m × 0.5 m and 0.4 m × 0.4 m, respectively. Modeling of a two-dimensions system was conducted using finite element software (SAP2000) to examine the inelastic seismic response of the base-isolated structure where ACI 318-19 code was followed for modeling the stiffness characteristics of beam' and columns' sections (ACI, 2019). Moreover, the appropriateness of retrofitting was investigated using equivalent lateral force following ASCE/SEI 7-16 (ASCE, 2016). Finally, three cases of the natural period of 2.15, 2.68, and 3 while three cases of damping ratio of 10%, 20%, and 30% to evaluate the efficiency of the QTFP isolator.

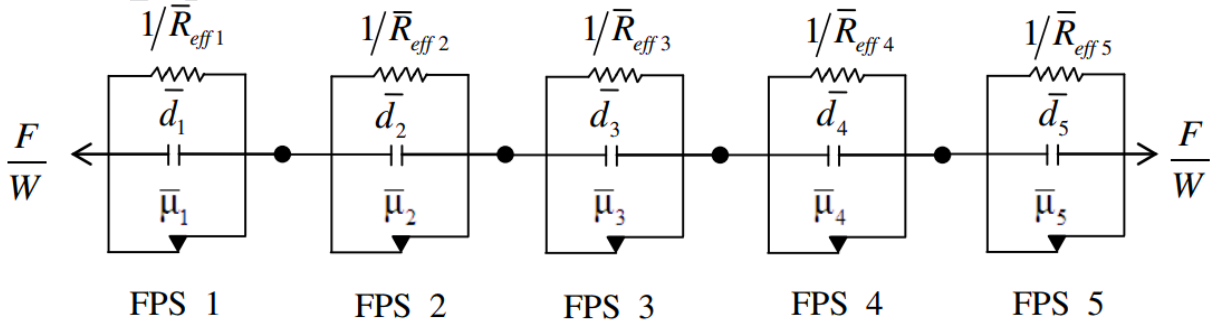

Figure 4: Numerical modeling of QTFP behavior (Lee and Constantinou, 2016)

Nonlinear time history analysis is a critical tool for understanding and predicting the structural behavior of buildings and other complex structures during seismic events. This computational procedure aims to forecast the dynamic response of structures to seismic loads. By incorporating time as an essential variable, it assesses the progressive changes in structural responses over a specific period. In the field of earthquake engineering, NLTHA is vital for modeling and testing the seismic performance of structures under real earthquake ground motions. It considers the relationship between stress and strain, accounting for the plastic behavior of materials under high-stress levels. This allows engineers to analyze potential structural deformations and evaluate seismic damage potential. The FEM approach plays a central role in NLTHA. FEM is a numerical technique that divides complex structures into numerous smaller, simpler parts, known as 'finite elements.' Each element can be analyzed for behavior under seismic loads, and when combined, they provide a detailed picture of how the entire structure will respond. The strength of the finite element approach lies in its versatility and precision. It can manage complex geometries, different types of materials, and varying boundary conditions, which make it uniquely suited for seismic load modeling. The model starts with defining the geometry of the structure, the properties of the materials used, and the applied loads or displacements. These variables, combined with the known laws of physics, allow us to solve for unknowns such as stress distributions, deformations, and natural frequencies. One of the critical aspects of this approach is the formulation of the nonlinear material models. Different construction materials, such as concrete, steel, or timber, respond differently to stress, strain, and high frequencies. These characteristics are integrated into the model, with each element assigned a specific material property. As the seismic load is applied, the model can predict nonlinear responses such as yielding or failure of the materials. Another fundamental aspect of the FEM in seismic load analysis is capturing the effect of the dynamic nature of earthquakes. Seismic waves can have a wide range of frequencies, and their effect on structures can change drastically depending on the frequency content. Therefore, an effective model should incorporate the dynamic characteristics of the structure, including its natural frequencies and mode shapes. The application of FEM in NLTHA is not limited

to buildings. It also extends to other structures such as bridges, dams, and tunnels. It helps in analyzing the effect of soil-structure interaction, a significant factor affecting the response of structures during earthquakes. By simulating the nonlinear behavior of soil and its interaction with the structure, engineers can develop more resilient designs. The development of a realistic and reliable structural model requires comprehensive understanding and application of validated methodologies. This report elaborates on the utilization of the National Institute of Standards and Technology (NIST) NIST GCR 17-917-46v3 guideline for the nonlinear modeling of a reinforced concrete (RC) frame superstructure in various models. Emphasizing the importance of accuracy and precision, this guideline was meticulously applied to address both material and geometric nonlinearity effects. The RC frames, by nature, are subjected to confinement effects that significantly influence the overall behavior of the structure. These effects were meticulously incorporated in our models through the application of the Mander et al. (1988) approach. This widely accepted method helped define the confined compressive stress-strain relationship of concrete, yielding more robust and accurate models. Besides, the behavior of concrete under tension was also accounted for, further enriching the comprehensive representation of the material's performance under varied conditions. In capturing the behavior of steel reinforcements, the Park and Paulay (1975) model, renowned for its ability to effectively represent the stress-strain response with symmetric compression and tension sections, was judiciously employed. The concrete compressive strength is 16 MPa and the steel yielding strength is 420 MPa. Th structural models boasted of three distinct fiber zones within the beam and column sections. These comprised the concrete cover, the concrete core, and the steel reinforcements, each modeled using separate approaches to ensure an in-depth and precise reflection of the structure's behavior. The outer concrete cover was modeled with unconfined concrete, the inner core with confined concrete, while the steel reinforcements were modeled in accordance with the approach proposed by Kalantari and Roohbakhsh (2020). A significant feature of our models was the employment of the fiber hinge model, a tool that effectively captures the nonlinear behavior of the structural elements. With this, the models transcended the realm of linear behavior, becoming capable of accurately predicting responses

under diverse and extreme loadings. This step was particularly crucial in understanding the structure's ultimate behavior and failure mechanism. Nonlinear time history analysis was then executed in SAP2000, deploying a direct integration approach. This methodology offered an insightful temporal exploration of the structural response, highlighting the time-varying nature of the structure's dynamic behavior. Guided by the approach presented in Kangda and Bakre (2018), the damping ratio in the superstructure was set at 2.5%. Notably, the first mode of the base isolated structure had its damping ratio overridden to zero to avert the phenomenon of damping leakage, a source of error often overlooked in such analyses. The damping leakage phenomenon in base isolated structures refers to the unintended addition of damping to the system's vibration modes. This occurs when utilizing classical or nonclassical damping models in finite element platforms to solve the equations of motion for base-isolated buildings. In the traditional damping matrix approach, the elastic stiffness of the system, including isolators, is considered. This method can inadvertently introduce damping to the first and higher vibration modes, leading to an unwarranted suppression of structural responses. The beam-column panel zone, a critical element that significantly influences the structure's overall deformation capacity, was modelled using line elements. These elements, conforming to NIST GCR 17-917-46v3, extended from the columns and beams towards the panel zone. This design contributed to a more realistic representation of the structure. Finally, the analysis incorporated the consideration of P-delta effects, pivotal in capturing the influence of gravity-induced forces on the structure's overall performance. However, the soil-structure interaction was intentionally neglected. Although it is generally considered in comprehensive models, this exclusion served to maintain a manageable complexity within the study's scope, focusing on the primary elements and their interactions.

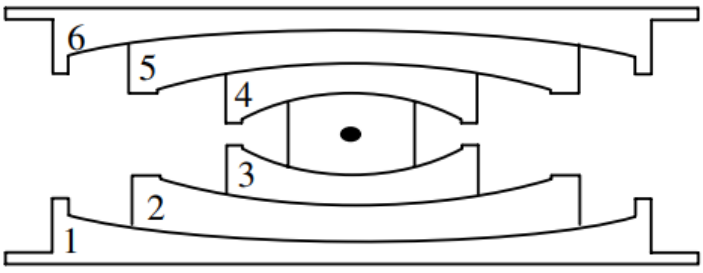

(a)

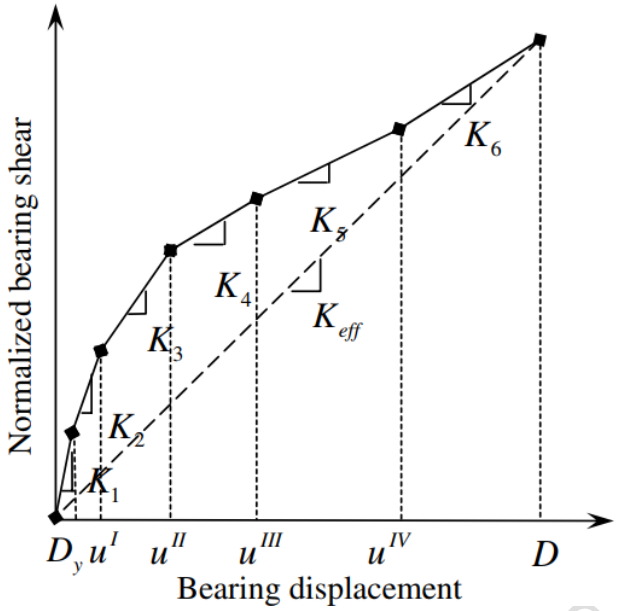

(b)

Figure 5: Calculation of the effective stiffness for QTFP as illustrated by Sodha et al. (2017)

The 1997 Umbria and Marche near-fault earthquake sequence was selected to conduct the study. The moment magnitude (M_w) scale for the foreshock record was recorded at the value of 5.7, while the mainshock exhibited M_w value of 6, and the aftershock record experienced M_w value of 5.5. Furthermore, the average shear wave velocity is up to 30 meters in depth (V_s30) was the same for the three cases of the earthquake, which are foreshock, mainshock, and aftershock, which eliminate the effect of changing the V_s30 parameters during the evaluation of these earthquakes on the efficiency and performance of the QTFP isolator. In fact, the Pacific Earthquake Engineering Research Center (PEER) was used in order to scale the sequence of near-fault earthquakes, as illustrated in Figure 6. The scaling approach followed in this study was a mean square error (MSE) where the three earthquake records were multiplied by a single scale factor. Lastly, 30 seconds of trailing zeroes were added at the end of the foreshock and mainshock earthquake records representing the time difference between the end of sequence foreshock and the beginning of sequence mainshock. At the end of the sequence aftershock earthquake record, 15 seconds of trailing zeroes were added to demonstrate the effect of the free vibration response of the structure (Kitayama and Constantinou, 2018).

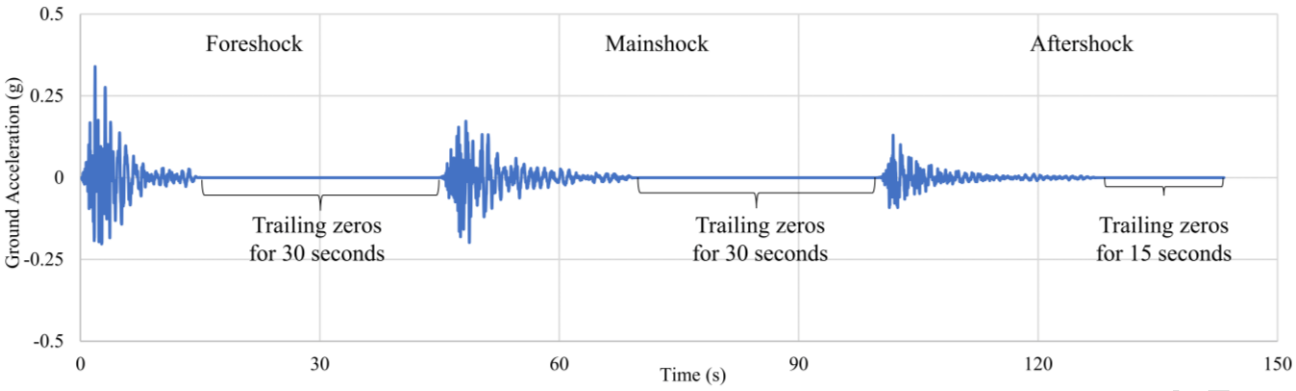

Figure 6: Developed sequence of foreshock, mainshock, and aftershock

3. Results and Discussions

This comprehensive evaluation aimed at understanding the seismic response of low-rise RC structures with an integrated MSFP isolator. The focus was primarily on how these structures would react under the influence of a series of near-fault foreshock, mainshock, and aftershock earthquakes. This sequence is often considered the most detrimental and damaging for structures due to the cumulative effect of the successive seismic events. Furthermore, the effectiveness and performance of the QTFP isolator, an innovative seismic isolation device, were also scrutinized under these earthquake sequences. Figure 7 in the report exhibited the time domain responses for the base shear of the structures under different earthquake records. The base shear essentially represents the total horizontal force in a building during an earthquake, and is a critical parameter in evaluating a structure's stability. An essential observation was the significantly high base shear time history response of the bare structure model – a structure without any form of base isolation. The bare model reported the highest values for the foreshock, mainshock, and aftershock earthquakes as compared to the cases where base isolation was employed. This comparison illuminated the benefits of utilizing base isolation techniques in low-rise RC structures. The results unequivocally highlighted that base isolation can be instrumental in managing the forces encountered during seismic events, thereby reducing the risk of structural damage or collapse. Another salient feature of the study was the exploration of different combinations of periods and damping ratios on the base shear response. The time-period of a structure is a fundamental attribute in structural dynamics and it is used to describe how a structure vibrates when it is excited. The damping ratio, on the other hand, is an indicator of

the energy dissipation capacity of a structure, which becomes particularly important during seismic events. The results illustrated that the combination of 2.15 seconds period and 10% damping ratio resulted in the highest base shear time history magnitudes. This was followed by the combination of 3 seconds period and 30% damping ratio, while the 2.68 seconds period and 20% damping ratio combination reported the lowest base shear magnitudes. These results could have significant implications for the design and construction of RC structures, specifically in seismically active regions. The data suggests that the performance of a structure during an earthquake can be significantly influenced by its period and damping ratio. The challenge for architects and engineers will be to determine the optimum combination of these variables to enhance the structure's ability to withstand seismic events. Additionally, the study revealed that the time history base shear values were recorded highest for all combinations and cases during the foreshock earthquake. This could be attributed to the fact that the foreshock earthquake, being the first in the sequence, tends to unsettle the structure, making it more susceptible to the subsequent seismic events. Finally, the bare structure model demonstrated the highest base shear value at 900 kN for the foreshock earthquake. This elevated value for the bare structure indicates the severe implications of omitting base isolation in design strategy.

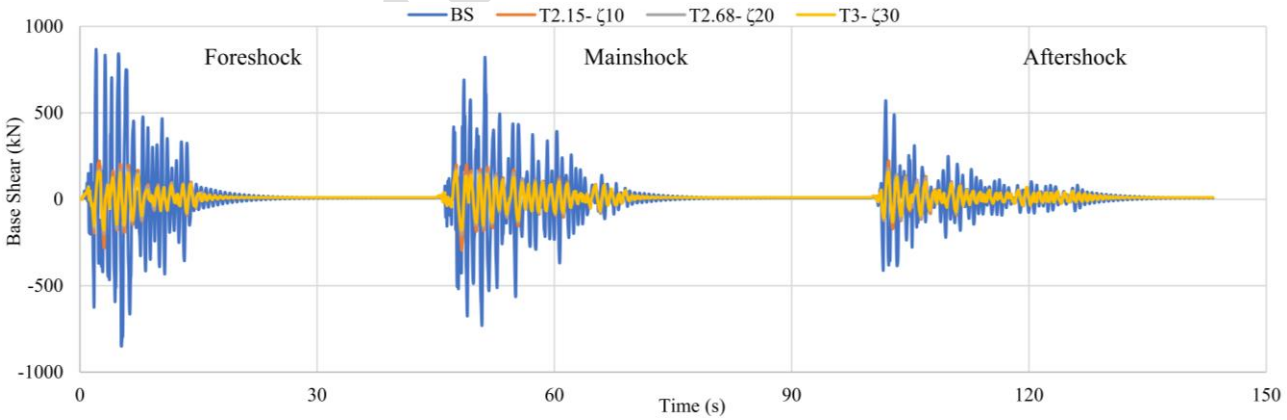

Figure 7: Base shear time history response

The study extended this analysis to a wide range of configurations to understand the behavior of the 3-story RC structure subjected to different earthquake events. It is noteworthy to mention that each earthquake type - foreshock, mainshock, and aftershock - represented unique force parameters in

terms of intensity, frequency, and direction. Consequently, the structure's response to these forces could significantly vary, leading to different stress and strain distributions, which in turn translated into varying story shear responses. The foreshock, as a preliminary tremor preceding the mainshock, had been selected for this analysis based on its high level of ground acceleration. Despite being considered a precursor, the foreshock was found to impose the highest demand on the building in comparison with the mainshock and aftershock. This finding could be attributed to the fact that the input force in the motion equation of a typical multi-degree of freedom system is a product of earthquake acceleration intensity and the building mass. As such, the highest shaking level of the foreshock induced the highest stress on the building. When it came to the base-isolated structures, the combination of specific damping ratio and period parameters made a significant difference in the structure's response. The optimal combination was found to be 2.15 seconds period and a 10% damping ratio, which triggered the highest story shear for the foreshock. This discovery demonstrates the potential of damping and period selection in alleviating seismic forces, offering designers a path to optimize the seismic resilience of their structures. Mainshock and aftershock analyses presented different results. Here, the highest story shear values were recorded in the combination of a 3 seconds period and a 30% damping ratio.

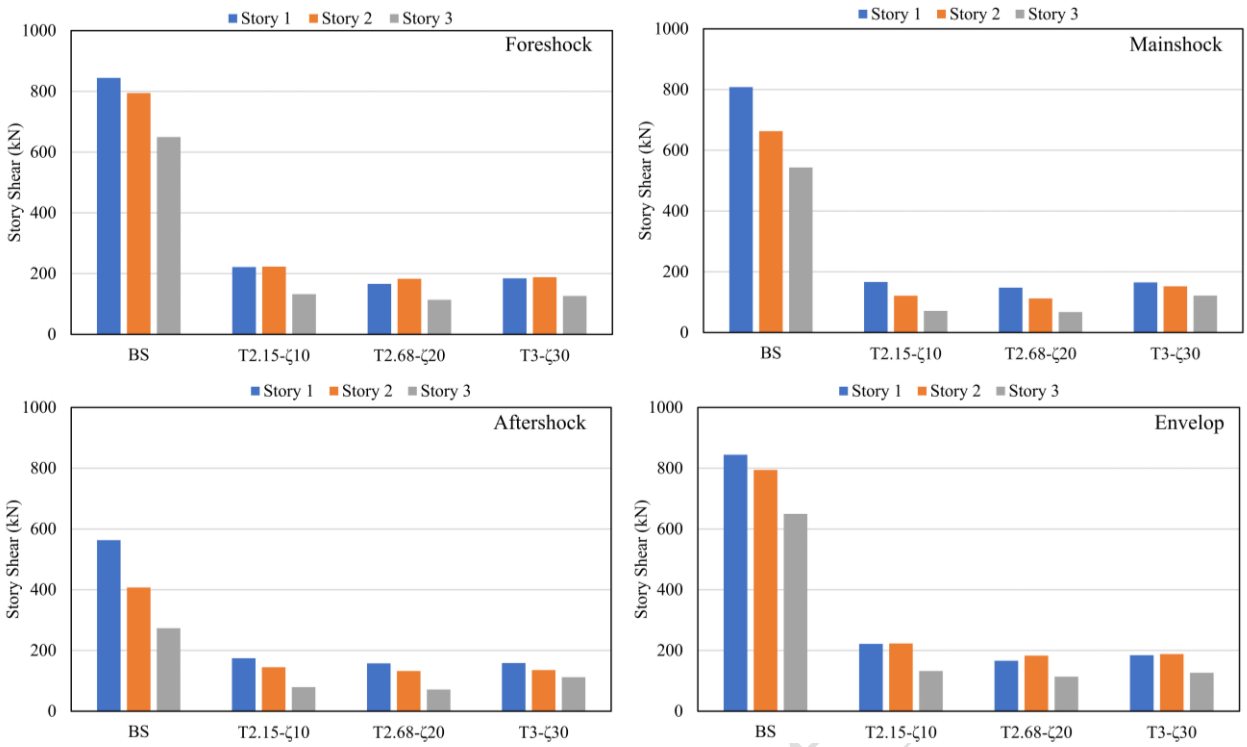

Figure 8: Story shear responses of the selected buildings

These configurations highlighted the dynamic nature of base isolation technology, proving its efficiency under a wide spectrum of seismic events, not just under the violent shaking of a mainshock, but also during the aftershock, which tends to have lower ground acceleration but can still significantly affect a building's stability. However, regardless of the earthquake type, it was observed that the first story consistently experienced the highest story shear magnitudes across all isolator property combinations. This trend is most likely due to the increase in load towards the base of the building, a phenomenon that is a fundamental aspect of statics and the field of structural engineering. It is often said that the first floor of a building bears the weight of the world, and this study confirms that assertion, especially when it comes to seismic loads. Following the first story, the second and third stories showed the next highest magnitudes, respectively. These results underscore the strain a multi-story building undergoes during seismic activity, with each level progressively sharing the burden of the one above. This cumulative effect is essential to consider when designing for earthquake resistance, ensuring that the structure's integrity is maintained at every level. This comprehensive analysis of story shear response sheds light on the complex interplay between building characteristics, isolator properties, and seismic event characteristics. It demonstrates how crucial it is to consider not

only the nature of the ground shaking but also the inherent structural properties of the building and the characteristics of the isolation system. It is clear that there is no one-size-fits-all solution to this complex problem. Instead, a nuanced approach that accounts for these different parameters will be necessary for the design of resilient buildings. QTFP isolator implemented with RC structures subjected to foreshock, mainshock, and aftershock earthquake records were investigated to examine these buildings' seismic behavior. Figure 9 represents the displacement time history response of the analyzed models. In general, the displacement response in the time domain of the bare structure reflected the highest magnitudes in contrast to base-isolated models. In base-isolated models, the displacement time history results were observed to be the highest in the combination of 2.15 seconds period and 10% damping ratio compared to 2.68 seconds period and 20% damping ratio as well as 3 seconds period and 30% damping ratio. The displacement time history response experienced the highest values for the bare structure model in the foreshock earthquake record, while the highest displacement results for the base-isolated models were seen in the case of the mainshock earthquake record. Lastly, the highest displacement time history value in the case of the bare structure was marked at 0.19 m, while the highest displacement result in the case of base-isolated models was recorded at 0.29 m.

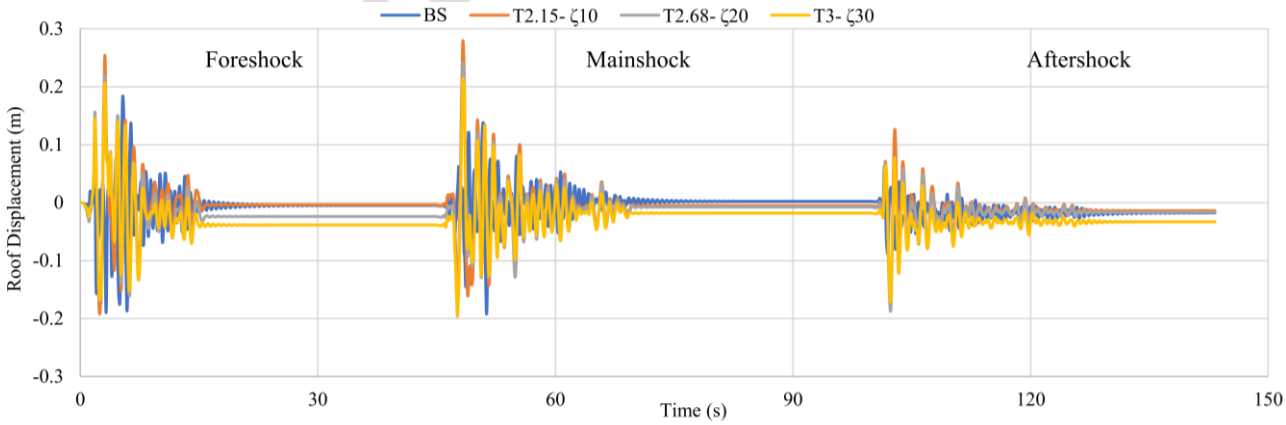

Figure 9: Displacement time history response

As can be observed, the inter-story drift ratio results of the 3-story RC structure equipped with a QTFP isolator are demonstrated in Figure 10. The inter-story drift response in the case of the foreshock earthquake record represented the highest values for the bare structure model. On the

contrary, the highest inter-story drift results for the base-isolated models were shown in the case of the mainshock earthquake record for all combinations at all story numbers. Furthermore, the highest inter-story drift results for the base-isolated models were recorded for the combination of 2.15 seconds period and a 10% damping ratio. The highest inter-story drift results were marked with the highest values in the first story for all cases and combinations under foreshock, mainshock, and aftershock earthquake records.

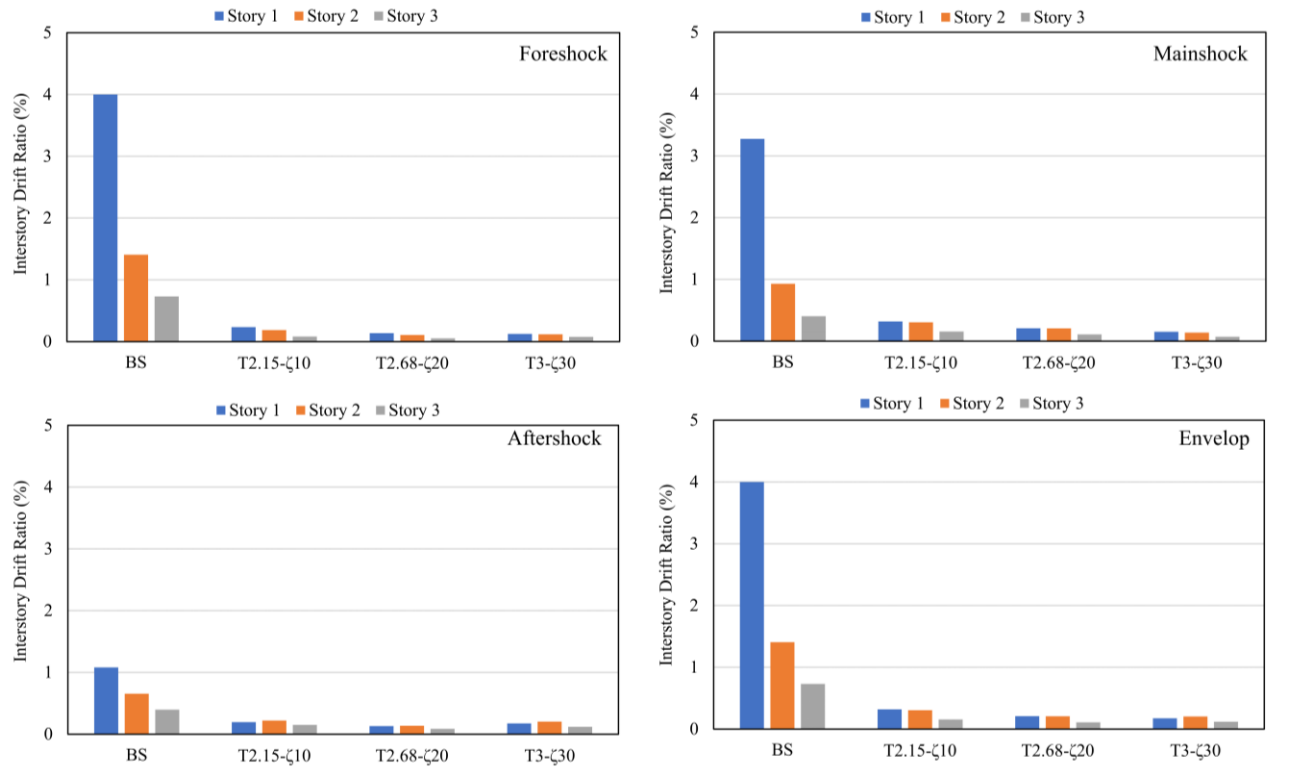

Figure 10: Inter-story drift ratios response of the selected buildings

The acceleration time history response of RC structures incorporated with a multi-staged friction pendulum isolator. The acceleration response in the time domain exhibited the highest results in the case of the bare structure model with respect to base-isolated structures, as illustrated in Figure 11. On the other hand, the highest acceleration response in the time domain for the base isolation system was generally recorded in the combination of a 2.15 seconds period and a 10% damping ratio representing the worst efficiency of the QTFP isolator in comparison to other combinations. The best performance of the QTFP isolator implemented with RC structures was seen in the combination of 3 seconds period and a 30% damping ratio, representing the lowest acceleration time history values. In

the case of the bare structure model, the highest acceleration time history values were observed for the foreshock earthquake record marking 25 $\frac{m}{s^2}$ while the highest acceleration results for the case of base-isolated models were shown in the foreshock earthquake, reaching 13 $\frac{m}{s^2}$.

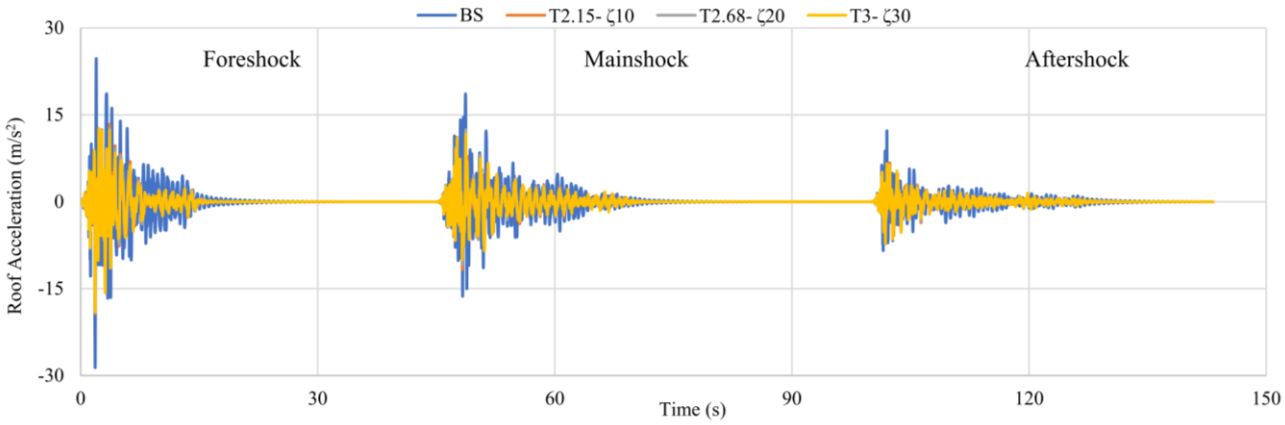

Figure 11: Accelerations time history response

The bare structure model displayed the highest story acceleration time history results in the case of foreshock earthquake, while the highest story acceleration values for the case of base-isolated models were seen in foreshock earthquake for all combinations at all number of stories as shown in Figure 12. In addition to that, the combination of 2.15 seconds period and a 10% damping ratio experienced the highest story acceleration response in the time domain. The story acceleration response recorded the highest magnitudes in the last story for foreshock and aftershock earthquake records, while mainshock earthquake expressed the highest story acceleration response in the second story for all combinations.

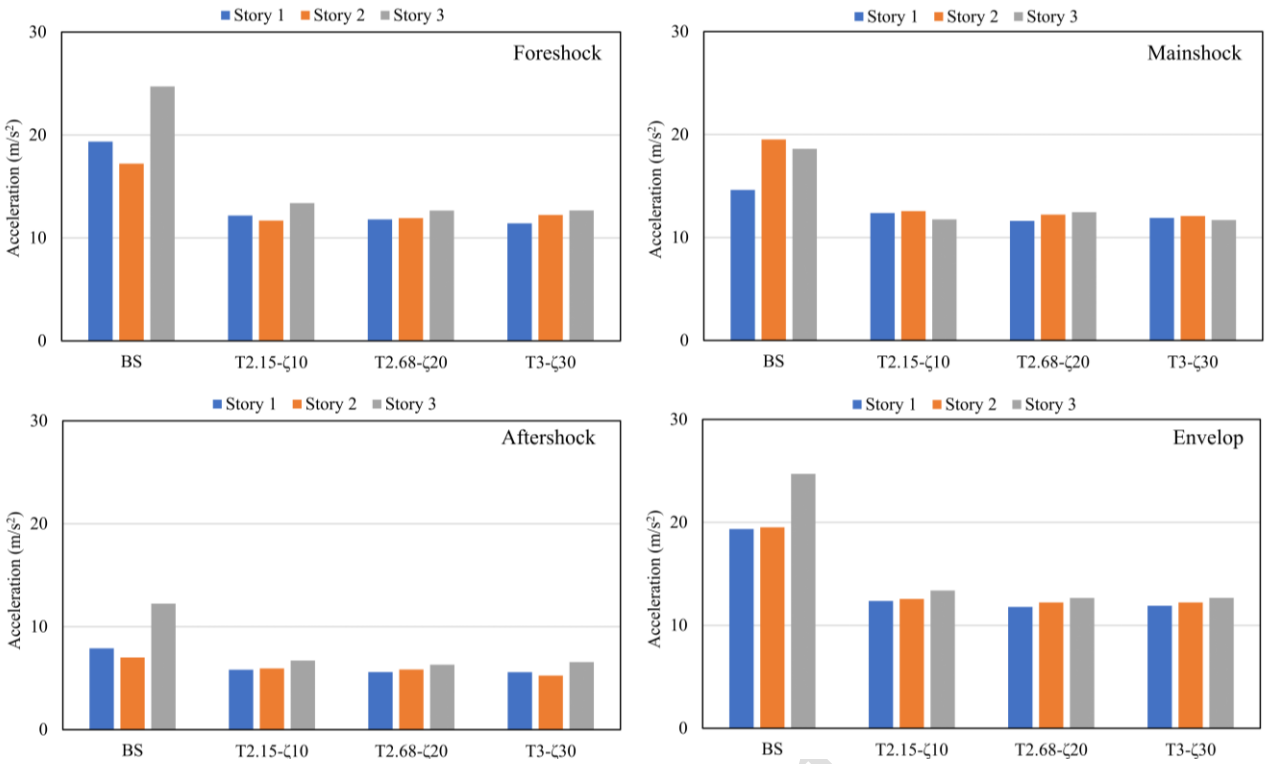

Figure 12: Story accelerations response of the selected buildings

The input energy time history response experienced the highest values in the case of the bare structure model in regard to base-isolated models, as represented in Figure 13. For the base-isolated structures, the highest input energy in the time domain was marked in the combination of 2.15 seconds period and a 10% damping ratio, while the lowest input energy values were seen in the combination of 3 seconds period and 30% damping ratio demonstrating the worst and best efficiency and performance of the multi-staged friction pendulum isolator respectively. The highest input energy for the bare structure model was experienced in the aftershock earthquake record at approximately 1050 kN.m. Moreover, the highest input energy results for the case of base-isolated buildings were displayed in the aftershock earthquake roughly at 930 kN.m.

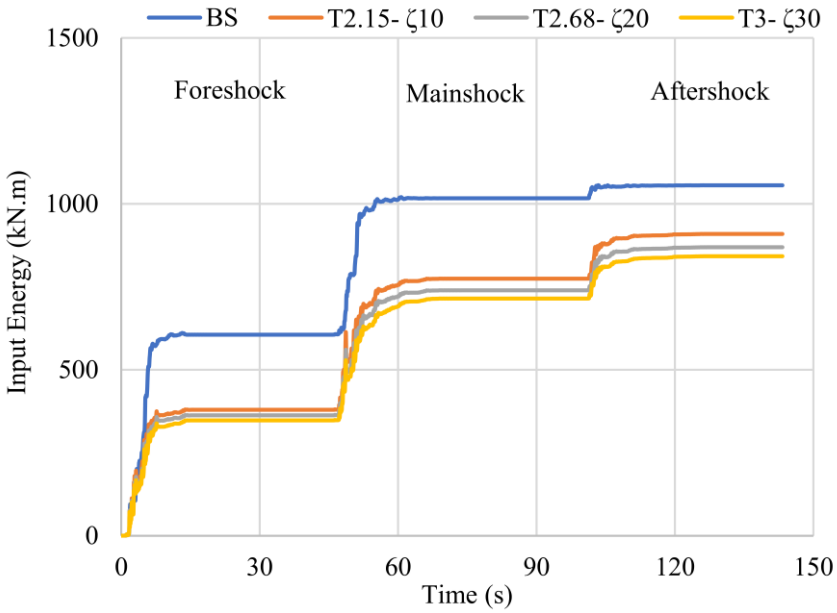

Figure 13: Input energy of the selected buildings

As can be seen in Figure 14, the kinetic energy response in the time domain was expressed the highest in the combination of 2.15 seconds and a 10% damping ratio representing the worst efficiency of the QTFP isolator compared to other buildings under the influence of sequence near-fault foreshock, mainshock, and aftershock earthquakes. Furthermore, the combination of 3 seconds and 30% damping ratio exhibited the lowest kinetic energy time history results, demonstrating the best base isolation system performance. Mainshock earthquake record showed the highest kinetic energy at an approximate value of 125 kN.m.

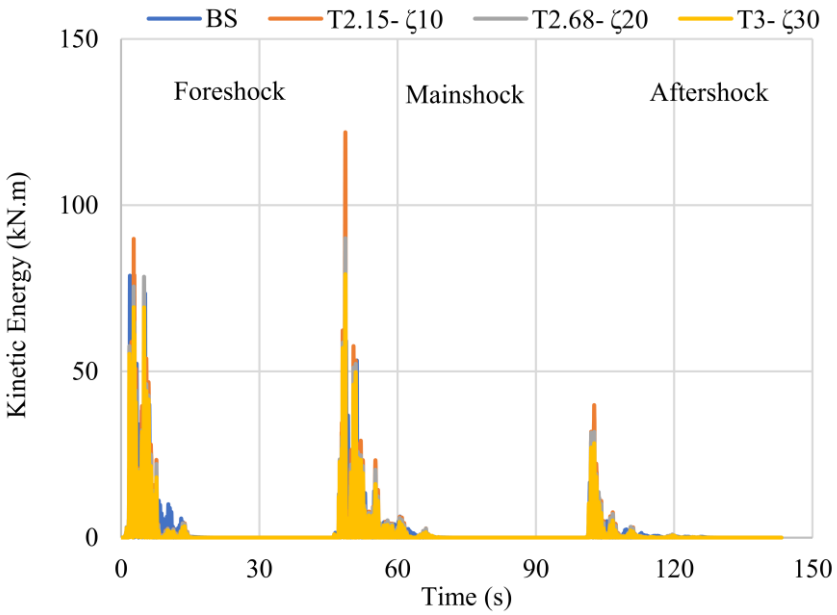

Figure 14: Kinetic energy of the selected buildings

The potential energy time history was observed to exhibit the highest results in the case of bare structure building in comparison to base-isolated models, as illustrated in Figure 15. Regarding base-isolated buildings, the highest potential energy in the time domain was recorded in the combination of 2.15 seconds period and a 10% damping ratio representing the worst efficacy of the base isolator. In addition to that, the lowest potential energy time history values were experienced in the combination of 3 seconds period and a 30% damping ratio representing the best efficiency of the QTFP isolator. The highest potential energy for the bare structure case was marked in the foreshock earthquake at 45 kN.m, while the highest potential energy value for the base-isolated case was expressed in the mainshock earthquake at 32 kN.m.

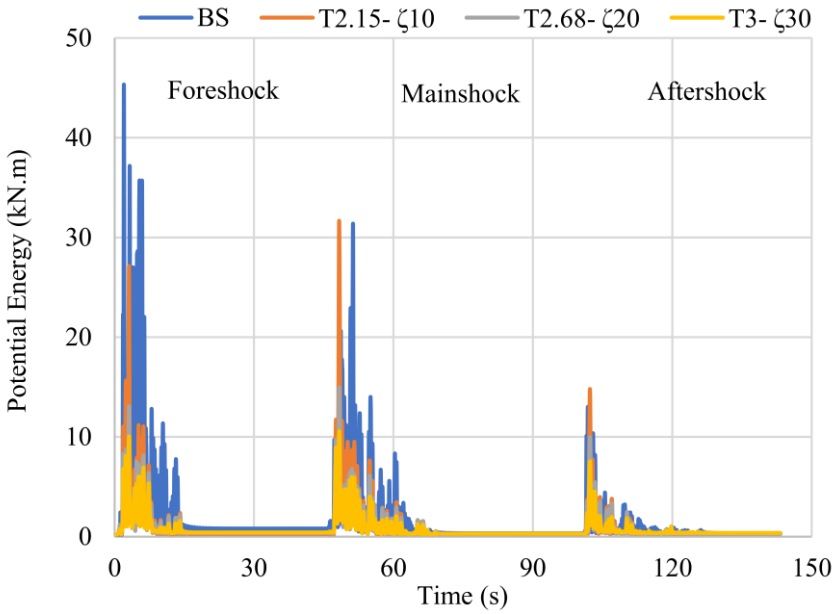

Figure 15: Potential energy of the selected buildings

The combination of 2.15 seconds period and a 10% damping ratio showed the highest damping energy time history response in contrast to the rest of the buildings, as represented in Figure 16. The lowest damping energy results were seen in the case of the bare structure model. The best performance of the multi-staged friction pendulum isolator equipped with RC structures was recorded in the combination of a 2.15 seconds period and a 10% damping ratio, while the lowest efficiency of the QTFP isolator was displayed in the case of bare structure building. The highest damping energy results for the bare structure model and all base-isolated models were exhibited in the case of the

aftershock earthquake record, where the highest damping energy in the case of the bare structure was observed at 210 kN.m. In comparison, the highest damping energy for the case of the base isolation system was experienced roughly at 520 kN.m.

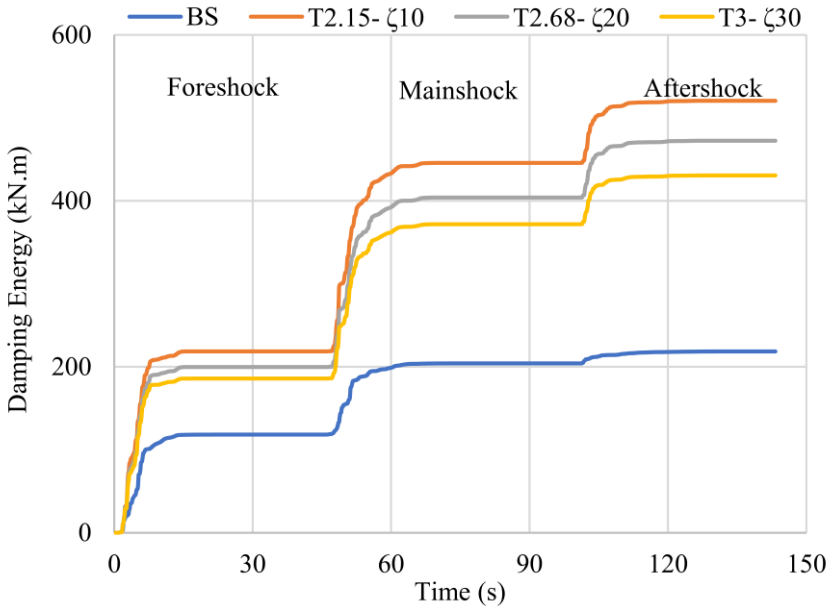

Figure 16: Damping energy of the selected buildings

As can be observed in Figure 17, the hysteretic energy of the RC structures incorporated with the QTFP isolator is represented. The highest hysteretic energy time history response was experienced in the case of bare structure building. On the contrary, the hysteretic energy in the time domain of the base-isolated models exhibited almost identical behavior regardless of the isolator properties. Finally, the highest hysteretic energy for the case of the bare structure model was seen at 830 kN.m, while the highest hysteretic energy for the base-isolated models was expressed at 410 kN.m.

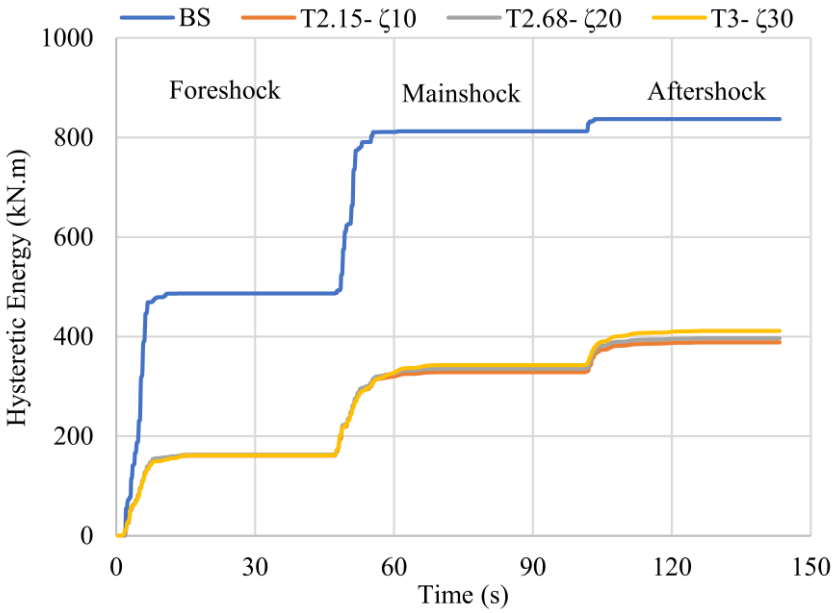

Figure 17: Hysteretic energy of the selected buildings

The importance of the hysteresis loop rises from the fact that it crucially impacts the seismic behavior of structures in regards to the analysis and design stages where the linear and nonlinear characteristics are demonstrated in relation to the damage. Figure 18 shows the hysteresis loop for the combination of 2.15 seconds period and a 10% damping ratio under the sequence of near-fault foreshock, mainshock, and aftershock earthquakes. The largest hysteresis loop cycle was observed in the case of the mainshock earthquake record, where the highest displacement value was found to be approximately 0.27 m, while the smallest hysteresis loop cycle was seen in the case of the aftershock earthquake, where the lowest displacement result was marked roughly at 0.13 m.

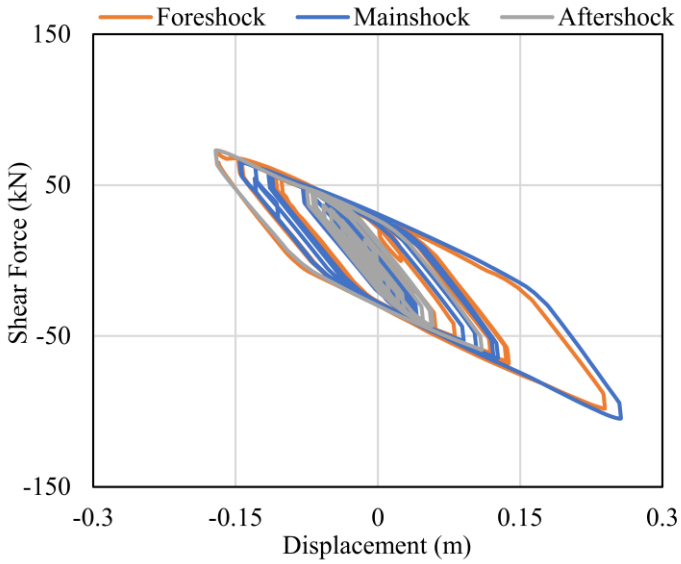

Figure 18: Isolator hysteresis behavior for the case of T2.15-ζ10

The largest hysteresis loop cycle for the combination of 2.68 seconds period and 20% damping ratio was experienced in the case of mainshock earthquake record, reaching the displacement result of 0.21 m representing the most significant damage on the QTFP isolator as illustrated in Figure 19. In addition, the smallest hysteresis loop cycle was exhibited in the case of an aftershock earthquake, where the lowest displacement response was found at 0.9 m demonstrating the least critical damage to the base isolation system.

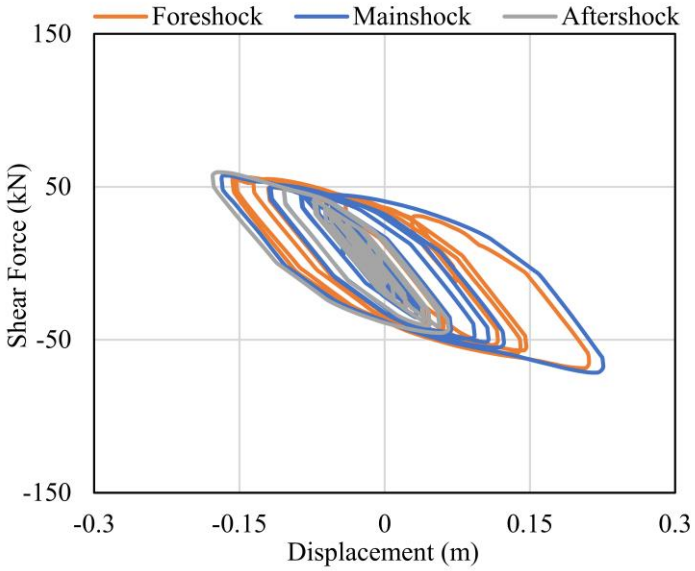

Figure 19: Isolator hysteresis behavior for the case of T2.68-ζ20

As can be observed in Figure 20, the hysteresis loop for the RC models utilized with a multi-staged friction pendulum isolator for the combination of 3 seconds period and a 30% damping ratio is represented. The mainshock earthquake record expressed the largest hysteresis loop cycle, where the highest displacement response was roughly at 0.18 m. Moreover, the smallest hysteresis loop cycle was experienced in the case of an aftershock earthquake, where the lowest displacement result was marked approximately at 0.7 m.

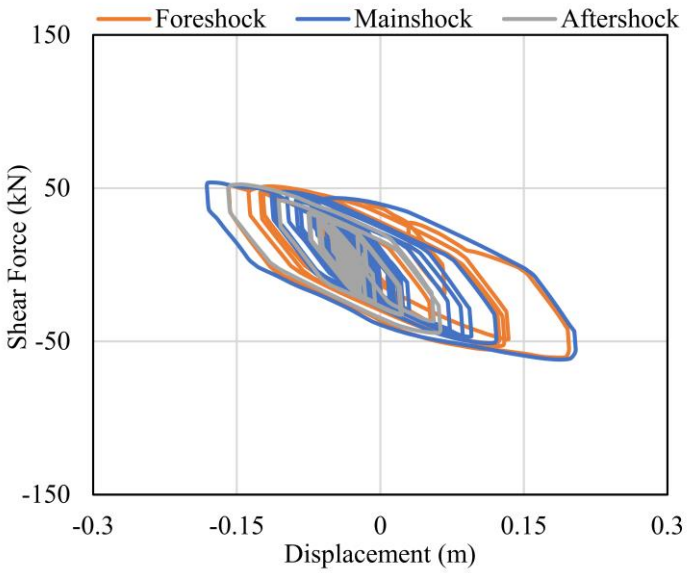

Figure 20: Isolator hysteresis behavior for the case of T3 -ζ30

The investigation of the efficiency and performance of the QTFP isolator implemented in RC structures was performed in terms of the structural responses, including base shear, acceleration, and inter-story drift, as shown in Table 2. The efficiency of the base isolation system was evaluated for each response in each case of the sequence of near-fault foreshock, mainshock, and aftershock earthquake records at each story of the 3-story model. The base shear results for the three combinations of isolator properties, which are 2.15 seconds period and 10% damping ratio, 2.68 seconds period and 20% damping ratio, as well as 3 seconds period and 30% damping ratio, were observed to exhibit the best performance of the isolator for all cases of earthquakes at all number of stories in the combination of 2.68 seconds period and 20% damping ratio. On the other hand, the worst performance of the QTFP isolator in terms of the base shear response was seen in the combination of a 2.15 seconds period and a 10% damping ratio. In addition to that, the acceleration response for the three stories generally expressed the best efficacy of the base isolation system in the combination of 3 seconds period and a 30% damping ratio for the three cases of earthquake loadings. At the same time, the worst performance of the isolator was recorded in the combination of 2.15 seconds period and a 10% damping ratio. Finally, the inter-story drift results for the three stories demonstrated the best efficiency of the isolator for the three cases of earthquake records in the combination of 2.68 seconds and a 20% damping ratio. In contrast, the worst performance of the

QTFP isolator for the three cases of earthquakes and all number of stories were displayed in the combination of 2.15 seconds period and a 10% damping ratio.

Table 2: Efficiency of the quintuple isolators in reducing building's responses under the sequence of earthquake loadings

Story Number	Earthquake Case	Base Shear			Acceleration			Interstory Drift		
		T2.15-ζ10	T2.68-ζ20	T3-ζ30	T2.15-ζ10	T2.68-ζ20	T3-ζ30	T2.15-ζ10	T2.68-ζ20	T3-ζ30
1	Foreshock	73.75	80.32	78.16	37.12	39.06	41.02	94.16	96.59	96.89
	Mainshock	79.40	81.70	79.58	15.36	20.58	18.60	90.26	93.64	95.38
	Aftershock	69.02	72.00	71.83	26.33	29.15	29.40	81.90	87.84	83.80
	Mean	74.06	78.01	76.53	26.27	29.60	29.67	88.77	92.69	92.02
2	Foreshock	71.92	76.94	76.31	32.12	30.79	28.99	86.75	92.37	91.60
	Mainshock	81.71	83.07	77.02	35.64	37.40	38.07	67.06	77.76	85.12
	Aftershock	64.45	67.47	66.77	15.27	16.67	25.08	66.21	79.17	68.93
	Mean	72.69	75.83	73.37	27.68	28.29	30.71	73.34	83.10	81.88
3	Foreshock	79.64	82.46	80.50	45.84	48.78	48.73	89.01	92.90	89.63
	Mainshock	86.85	87.61	77.62	36.83	33.09	37.18	61.42	72.91	82.52
	Aftershock	70.91	73.91	59.01	45.14	48.48	46.31	62.32	78.08	69.87
	Mean	79.13	81.32	72.37	42.60	43.45	44.07	70.92	81.30	80.67
Low efficiency										High efficiency

4. Conclusion

The focus of this study was an exploration into the seismic behavior of low-rise RC models when equipped with a QTFP isolator. All possible isolator properties were considered under a sequence of near-fault foreshock, mainshock, and aftershock earthquake events. The study also investigated how these earthquake events influenced the structural responses of the base-isolated RC buildings. A performance evaluation of the QTFP isolator in conjunction with RC structures subjected to sequences of near-fault earthquakes was conducted, and the results were compared against a benchmark model of a bare structure. On the basis of the research presented in this study, it can be concluded that:

- The RC models integrated with the QTFP isolator have effectively reduced the responses of base-isolated structures, displaying adequate performance.

- The QTFP isolator showed maximum efficiency in terms of base shear and inter-story drift when combined with a 2.68 seconds period and a 20% damping ratio. However, the combination of a 3 seconds period and a 30% damping ratio demonstrated the highest performance for the acceleration response in the base isolation system.
- The sequence of near-fault earthquakes, including foreshock, mainshock, and aftershock events, has a significant influence on the studied structural response. The foreshock event resulted in the greatest values of base shear, inter-story drift, and acceleration responses for both the bare and base-isolated models.
- The record of the aftershock earthquake demonstrated the highest input, damping, and hysteretic energies for both the unadorned structure and the base-isolated buildings.
- The hysteresis behavior of the isolator was noted during the mainshock earthquake record for the three QTFP isolator combinations. Among all the instances, the combination of a 2.15 seconds period and a 10% damping produced the largest cycles of the hysteresis loop.

In conclusion, this study was limited to analyzing a single natural sequence of motion due to the lack of many causes existing in reality. Other studies in the literature can focus on comparing natural and artificial sequences of motion and their capabilities in capturing the true response of base-isolated structures when subjected to long seismic loadings.

Conflicts of Interest

On behalf of all the authors, the corresponding author states that there is no conflict of interest.

References

ACI. (2019). *ACI 318-19: Building Code Requirements for Structural Concrete and Commentary*, Farmington Hills, USA: American Concrete Institute.

ASCE. (2022). *ASCE/SEI 7-22 Minimum Design Loads For Buildings and Other Structures.*

Constantinou, M., Mokha, A., and Reinhorn, A. (1990). "Teflon bearings in base isolation II: Modeling", *Journal of Structural Engineering, 116*(2), 455-474.

CSI. (2022). "SAP2000 version 22 - Structural Software for Analysis and Design", *California: Computers and Structures Inc*.

Dhankot, M. A., and Soni, D. P. (2017). "Behaviour of triple friction pendulum isolator under forward directivity and fling step effect", *KSCE Journal of Civil Engineering, 21*(3), 872-881.

Fenz, D. M., and Constantinou, M. C. (2006). "Behaviour of the double concave friction pendulum bearing", *Earthquake engineering and structural dynamics, 35*(11), 1403-1424.

Gandelli, E. (2017). *Advanced tools for the design of sliding isolation systems for seismic-retrofitting of hospitals*, Milan, Italy: Politecnico di Milano.

Kalantari, A., and Roohbakhsh, H. (2020). "Expected seismic fragility of code-conforming RC moment resisting frames under twin seismic events", *Journal of Building Engineering, 28*, 101098.

Keikha, H., and Ghodrati Amiri, G. (2021). "Numerical development and assessment of 3D quintuple friction pendulum isolator element based on its analytical and mathematical models", *Journal of Earthquake Engineering, 25*(13), 2718-2757.

Keikha, H., and Ghodrati Amiri, G. (2021). "Seismic performance assessment of quintuple friction pendulum isolator with a focus on frictional behavior impressionability from velocity and temperature", *Journal of Earthquake Engineering, 25*(7), 1256-1286.

Kitayama, S., and Constantinou, M. C. (2018). "Seismic Performance of Buildings with Viscous Damping Systems Designed by the Procedures of ASCE/SEI 7-16", *Journal of Structural Engineering, 144*(6), 04018050.

Lee, D., and Constantinou, M. C. (2016). "Quintuple friction pendulum isolator: Behavior, modeling, and validation", *Earthquake Spectra, 32*(3), 1607-1626.

Mander, J. B., Priestley, M. J., and Park, R. (1988). "Theoretical stress-strain model for confined concrete", Journal of structural engineering, 114(8), 1804-1826.

Mesr Habiby, Y., and Behnamfar, F. (2023). "Seismic fragility analysis of torsionally-coupled steel moment frames against collapse", *Civil Engineering Infrastructures Journal*.

Mirrashid, M., and Naderpour, H. (2021). Innovative computational intelligence-based model for vulnerability assessment of RC frames subject to seismic sequence. *Journal of Structural Engineering*, *147*(3), 04020350.

Mokha, A., Constantinou, M. C., Reinhorn, A. M., and Zayas, V. A. (1991). "Experimental study of friction-pendulum isolation system", *Journal of Structural Engineering*, *117*(4), 1201-1217.

Mokha, A., Constantinou, M., and Reinhorn, A. (1990). "Teflon bearings in base isolation I: Testing", Journal of Structural Engineering, 116(2), 438-454.

Naderpour, H., Naji, N., Burkacki, D., and Jankowski, R. (2019). Seismic response of high-rise buildings equipped with base isolation and non-traditional tuned mass dampers. *Applied Sciences*, *9*(6), 1201.

Nallasivam, K. (2023). "Effective Location of Shear Walls in High-Rise RCC Buildings Subjected to Lateral Loads", *Civil Engineering Infrastructures Journal.*

NIST. (2017). *Guidelines for Nonlinear Structural Analysis for Design of Buildings Part IIb – Reinforced Concrete Moment Frames,* National Institute of Standards and Technology.

Park, R., and Paulay, T. (1975). *Reinforced Concrete Structures.* Wiley .

Sarlis, A. A., and Constantinou, M. C. (2013). *Model of triple friction pendulum bearing for general geometric and frictional parameters and for uplift conditions,* University at Buffalo, Buffalo, NY: Technical Report MCEER-13-0010, Multidisciplinary Center for Earthquake Engineering Research.

Sharbatdar, M. K., Vaez, S. H., Amiri, G. G., and Naderpour, H. (2011). Seismic response of base-isolated structures with LRB and FPS under near fault ground motions. *Procedia Engineering*, *14*, 3245-3251.

Sodha, A. H., Soni, D. P., and Vasanwala, S. A. (2021). "Evaluation of linear visco-elastic model of quintuple friction pendulum isolator", *International Journal of Structural Engineering*, 11(1), 19-43.

Sodha, A. H., Soni, D. P., Desai, M. K., and Kumar, S. (2017). "Behavior of quintuple friction pendulum system under near-fault earthquakes", *Journal of Earthquake and Tsunami*, *11*(5), 1750017.

Tsai, C. S., Lin, Y. C., and Su, H. C. (2010). "Characterization and modeling of multiple friction pendulum isolation system with numerous sliding interfaces", *Earthquake engineering and structural dynamics*, *39*(13), 1463-1491.

Zayas, V. A., Low, S. S., and Mahin, S. A. (1987). *The fps earthquake resisting system: Experimental report (ucb/eerc-87/01),* Berkeley, CA: University of California.